ACS Photonics

Article

pubs.acs.org/journal/apchd5

Coupled T-Shaped Optical Antennas with Two Resonances Localized in a Common Nanogap

Katja Dopf,*[,†,‡] Carola Moosmann,*[,†,‡] Siegfried W. Kettlitz,[†] Patrick M. Schwab,[†,¶] Konstantin Ilin,[§] Michael Siegel,[§] Uli Lemmer,[†,¶] and Hans-Jürgen Eisler*[,†]

[†]Light Technology Institute (LTI), Karlsruhe Institute of Technology (KIT), Kaiserstraße 12, D-76131 Karlsruhe, Germany

[¶]Institute of Microstructure Technology (IMT), Karlsruhe Institute of Technology (KIT), Hermann-von-Helmholtz-Platz 1, D-76344 Eggenstein-Leopoldshafen, Germany

[§]Institute of Micro- and Nanoelectronic Systems (IMS), Karlsruhe Institute of Technology (KIT), Hertzstraße 16, D-76187 Karlsruhe, Germany

S *Supporting Information*

ABSTRACT: Resonant optical antennas with nanoscale gaps are of high interest due to their ability to enhance electric fields in localized subdiffraction-limited volumes. They are especially attractive for coupling with quantum emitters. One challenge for applications that exhibit a spectral shift is to fabricate nanoantennas that provide two distinct resonances at the excitation and emission frequency, respectively. We propose a coupled T-shaped nanoantenna structure that provides independently controllable resonances with a common electromagnetic hot spot in the antenna gap. We demonstrate the fabrication of such structures and investigate experimentally and theoretically their spatial, time-integrated spectral- and polarization-dependent electromagnetic field properties. The nanoantennas exhibit two resonances with unique spectral and polarization responses. The resonance wavelengths are independently tailored by varying the geometry of individual T-shaped antennas.

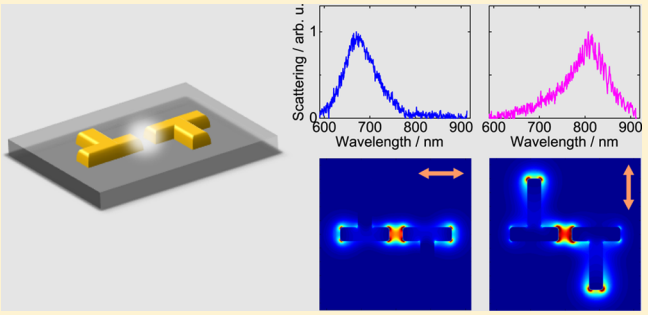

KEYWORDS: *Nanoantenna, particle plasmon resonance, plasmonics, dark-field spectroscopy, FDTD simulations*

In the past decade resonant optical antennas[1] have attracted huge interest for their unique properties in controlling light at a subwavelength scale. Optical antennas are nanometer-scale structures that efficiently mediate between freely propagating radiation and highly localized near-fields.[2−5] Their particle plasmon resonances (PPRs) highly depend on the material composition, the (complex) dielectric function of the environment shape, and the interaction of an individual antenna with neighboring nanoparticles, including near-field and far-field interaction.[6] Coupled nanoantennas composed of antenna arms separated by a nanometer-sized gap offer several attractive properties[7−9] such as the extremely high fields in the hot spot.

Antenna applications range from optical sensing and energy harvesting[10−12] to a control of the fluorescence of single emitters,[13−16] super-resolution microscopy,[17] and nonlinear plasmonics.[18,19] Several applications require antenna geometries with bimodal or multimodal spectral properties. Among those are frequency mixing nonlinear optical methods such as higher harmonic generation[20−26] and difference frequency generation.[27] Another area of application focuses on controlling the near- and far-field properties of the polarization. Bimodal optical antennas have been proposed for manipulating the polarization state in the near-field of a nanoantenna.[28−30] In this context, plasmonic waveplates have been demonstrated.[29,31] For polarization control applications, the two resonance wavelengths can also be identical. Such antenna structures can preserve the far-field polarization in the near-field.[32,33] Multiresonant structures have also been proposed as color sorters.[34−36] Another growing field of research focuses on the excitation of Fano resonances,[37] which can also exploit bimodal antenna structures.[38−42] Finally, multiresonant or broadband nanoantenna arrays have been applied for light trapping for example in solar cells.[43−45] The structure presented here is promising for these applications.

In the applications mentioned before different multiresonant nanoantenna geometries have been used. These include gap dipole antennas with different arm lengths,[46,47] log-periodic structures,[22,48,49] L-shaped nanostructures in different arrangements,[23,31,50] asymmetric bowtie antennas,[34,36] single T-shaped antennas,[20,26,38−41] bimetal antennas,[35] a V-shaped antenna coupled with a nanorod,[25] and cross-shaped optical gap antennas.[27−30,32,33,43−45,51−53]

Received: August 7, 2015
Published: October 12, 2015

DOI: 10.1021/acsphotonics.5b00446
ACS Photonics 2015, 2, 1644−1651

Within this work we focus on a design for bimodal antenna structures that show enhanced excitation capabilities and independently tunable emission properties for quantum emitters (QEs) placed in a single antenna hot spot. It has been extensively studied how hybrid coupled nanoantenna−QE systems can have properties superior to pure QEs.[54,55] The positive effects of the antenna on the emitter include enhanced scattering or absorption cross sections[56] and a high directionality.[57−59] By tuning the PPR of the antenna the desired channel can be optimized and the coupling effects can be exploited and studied. In contrast to conventional radio antennas, which are usually electrically connected, optical antennas are most commonly optically driven. Consequently, antenna−QE systems are optically excited, and the reemitted response signal is likewise optically detected. Since QEs exhibit a significant Stokes shift between absorption and emission, nanoantennas for coupling with QE systems ideally support two resonances. Accordingly, for a profound understanding of the contributing effects a separation of the absorption and emission process is advantageous, which has not been presented so far.

Despite the huge amount of nanoantenna research, only a few previous works focused on double-resonant structures for enhanced absorption and emission.[47,53,60] Therefore, we have realized a novel structure, the coupled T-shaped nanoantenna, which meets all of the following requirements: (i) the antenna supports two resonances, (ii) high field enhancements for both modes are supported in the same nanometer-scale hot spot, (iii) the resonance wavelengths can be chosen independently of each other by varying the geometry, (iv) the structure allows for discrimination between the resonance modes based on both polarization and wavelength.

Since the above summarized variety of antenna geometries are designed for different kinds of applications, they do not meet all these requirements perfectly. The cross-shaped antenna (four antenna arms sharing a common nanogap) is the closest to the structure presented here. However, the biggest challenge of this structure is to design and fabricate a nanogap so that high field enhancements can be achieved and coupling of nearest neighboring arms is avoided.[28,32,53] Furthermore, the design of Celebrano et al.[25] combines the control of the two resonances involved in second-harmonic generation with the required asymmetry. Yet this structure is very specialized for this particular application. The presented coupled T-shaped optical antenna overcomes the challenges of these architectures and complements the features of other candidates. It provides a very promising design for applications requiring bimodal resonances.

RESULTS AND DISCUSSION

T-Shaped Antenna Design. Here we present an antenna design consisting of coupled T-shaped gold antennas that are separated by a nanoscale gap. Figure 1 provides a schematic of the T-shaped antenna. The structure supports two resonances in the visible wavelength range at perpendicular polarization angles. Two dipole gap antennas arranged perpendicular to each other (cross-shaped antennas) represent a simple method to realize two resonant modes. Here, we modify this geometry and connect these two dipole gap antennas to form a structure with improved gap coupling properties.

The T-shaped antenna can be viewed as an established dipole gap antenna where an additional bar is attached to each antenna arm forming the letter "T". We call the two bars of the "T" top t and base b (see Figure 1). The first resonance can be tuned by changing the top length t similar to a dipole antenna.[8,61] The second antenna resonance is mainly defined by the length of the attached base b. Attaching the base at (or close to) the middle position and not at the ends of the top arm assures the highest degree of independence between the two modes. This goes along with the findings of Prangsma et al.[62] In contrast to the here presented bimodal T-shaped antenna, they demonstrated a similar structure where the (very long) base is not used to define a second mode, but for electrically connecting the dipole gap antenna part without perturbing the optical performance of the dipole. Using our design, both optically active resonances are supported in an individual optical antenna and share the same nanogap. By considering fabrication limitations accomplishable resonance wavelengths depend mainly on the geometrical parameters. To achieve a useful top resonance, the top length has to be significantly larger than the width of the antenna base. This minimum top length defines the smallest possible resonance wavelength, whereas there is no equivalent upper limit for the long resonance wavelength. The huge benefit of the T-shaped gap antenna is the controllable separation of two distinct eigenmodes within the same structure and in the antenna hot spot by polarization. While the coupling of two single "T" structures will generate optically active as well as inactive (so-called dark) plasmon eigenmodes, we restricted ourselves to the optically active antenna modes.

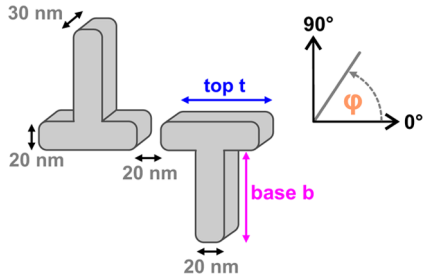

Figure 1. Schematic of the T-shaped nanoantenna with geometrical parameters. The width and gap size is fixed to 20 nm, the top length t is varied from 50 to 90 nm, and the base length b varies from 0 to 90 nm. The polarization angle is defined as shown by φ.

Near-Field and Far-Field Properties of a Coupled T-Shaped Nanoantenna. The working principle of the coupled T-shaped structure is presented here for an antenna with a top and base length of 70 nm each. Far-field scattering measurements in combination with near-field simulations at the two resonance wavelengths give a profound insight in the characteristics of the antenna. Figure 2A shows the measured dark-field scattering spectra for this T-shaped nanoantenna. The first resonance for light polarized along the top ($\varphi = 0°$) has its peak at $\lambda_{top} = 677$ nm, while the second resonance at $\lambda_{base} = 807$ nm can be seen for light polarized along the base ($\varphi = 90°$). Thus, the design criterion of two resonances that differ in wavelength and also in polarization is satisfied.

The precise properties of the two modes can be further understood by investigating the near-field. Here we present finite-difference time-domain (FDTD) simulations to examine the near-field enhancement as well as the current density in the antenna. The near-field peak resonance wavelengths were calculated in the middle of the antenna gap, and they are at $\lambda_{top,near} = 711$ nm for an angle $\varphi = 0°$ and at $\lambda_{base,near} = 864$ nm for $\varphi = 90°$. The field enhancement in the antenna gap

DOI: 10.1021/acsphotonics.5b00446
ACS Photonics 2015, 2, 1644−1651

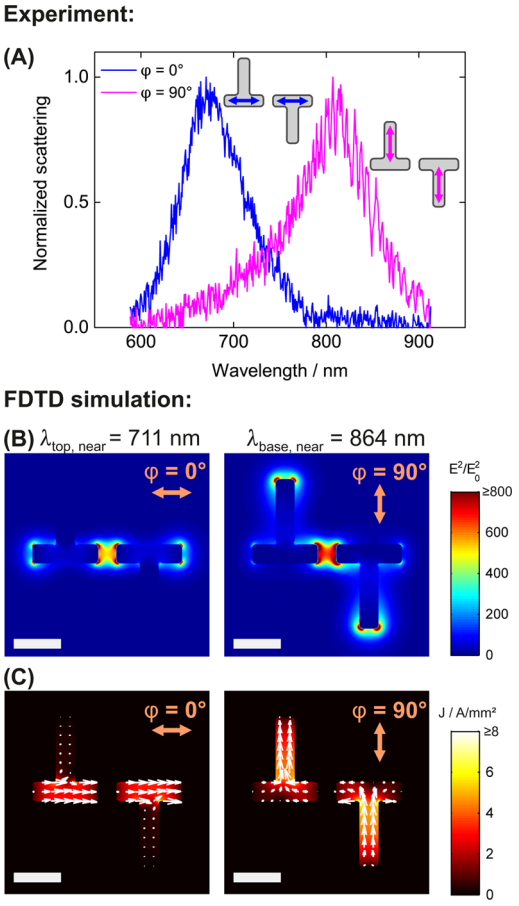

Figure 2. Far-field and near-field properties of a T-shaped antenna with top length t = 70 nm and base length b = 70 nm (scale bar 50 nm). (A) Dark-field scattering measurements for polarization along the top (φ = 0°) and along the base (φ = 90°) of a single T-shaped gap antenna. (B and C) Near-field FDTD simulations for polarization along the top ($\lambda_{top,near}$ = 711 nm, φ = 0°) (left images) and polarization along the base ($\lambda_{base,near}$ = 864 nm, φ = 90°) (right images): (B) electric field enhancement E^2/E_0^2 and (C) current density distribution J at half the antenna height.

depending on the wavelength and the polarization angle is shown in detail in the Supporting Information (Figure S1).

It is important to note that, first, there is a small shift in the resonance wavelength between the (simulated) far-field and (simulated) near-field, which is well known and extensively studied.[63] Second, the resonance wavelength of the measured far-field scattering signal differs from the simulated scattering resonance wavelength. We can clearly attribute the major part of the difference in peak resonance wavelength between experiment and simulation to the challenge of making sharp inner edges using electron beam lithography. Corresponding simulation results with adapted geometries are shown at the end of the paper.

Figure 2B and C show the simulated electric fields and current densities at half the antenna height. As intended, the electric field enhancements in the gap (Figure 2B) are extremely high (approximately 500× enhancement) for both antenna modes. Hence our structure also fulfills the design criterion of a common hot spot for both resonances. The strength of the field enhancement for both modes is very close to the enhancements observed in dipole nanoantennas. Generally, with smaller gap sizes even higher field enhancements are possible, but the fabrication is more challenging. It is worth noting that the near-field polarization in the gap is along the antenna top direction for both modes, although the far-field polarizations are perpendicular to each other. This is further supported by adding the in-plane component of the electric field vectors in the near-field intensity plots in the Supporting Information (see Figure S2). This property contrasts with other bimodal geometries, for example that of the cross-shaped antennas, and can be advantageous for several applications. If the orientation of a dipole emitter can be controlled, the dipole can couple optimally in terms of absorption and emission, assuming that the absorption and the emission dipole moments of the single QEs are parallel to each other. Besides the field enhancement in the gap a smaller field enhancement at the antenna ends not facing the gap can be observed, indicating where the plasmon mode is located. For the first antenna mode at an angle of φ = 0° the fields close to the antenna top ends are enhanced; for the second antenna mode at an angle of φ = 90° the fields close to the antenna bases are enhanced. Furthermore, when looking at the current density distribution (Figure 2C) in the antenna arms the plasmon oscillation modes can directly be determined by the amplitude and vector representation. For the top resonance the current distribution on the top antenna arms looks very similar to that of a pure dipole gap antenna, with a small disturbance in the center of the individual arms due to the base. The current flow along the base is approximately zero. In contrast, for the second antenna mode, the current mode distribution shows that the particle plasmon oscillation mainly arises along the base and turns around the corner toward the antenna gap, but also a lower current flow can be observed in the top toward the ends not facing the gap.

Polarization Dependency of the Antenna Eigenmodes. Thus far, we concentrated on the two polarization angles φ = 0° and φ = 90°. We further investigated the scattering signal at the two far-field resonance wavelengths in dependence on the polarization angle to determine the weighting of the two modes.

In Figure 3 we show the scattering depending on the polarization for simulation (λ_{top} = 707 nm and λ_{base} = 862 nm) and for the experiment (λ_{top} = 677 nm and λ_{base} = 807 nm) of the top and the base resonance at different angles (T-shaped antenna with t = 70 nm and b = 70 nm). The resonances were normalized to the maximum of the long wavelength mode in

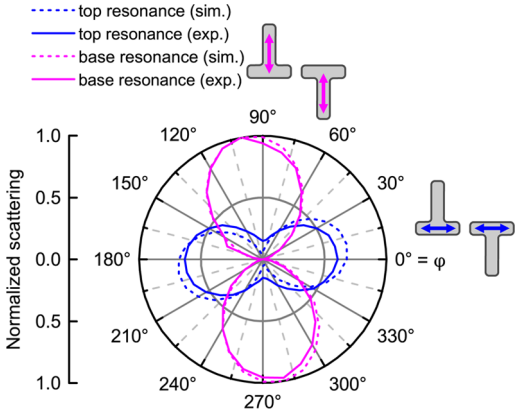

Figure 3. Normalized scattering depending on the polarization angle φ for the two modes at λ_{top} = 707 nm and λ_{base} = 862 nm for the simulation and λ_{top} = 677 nm and λ_{base} = 807 nm for the experiment.

DOI: 10.1021/acsphotonics.5b00446
ACS Photonics 2015, 2, 1644−1651

order to qualitatively compare the results. The scattering signals show a $\cos^2$ dependency on the polarization angle (see also Supporting Information Figure S5). The optimal polarization angles for the two modes are not exactly at 0° and 90°. For this particular antenna geometry, for example, the top resonance is best excited with an incident wave polarized at an angle of 8° and the second mode, which is associated with the base of the T-shaped antenna, has an optimal polarization angle at 97°. The slight shift in the angle originates from the coupling of the two T-shaped antenna arms. At these particular angles there is no cross-talk into the other mode, and they are best separated. Alternatively to adjusting the polarization angle, the point of base attachment can be shifted from the middle of the top slightly toward the gap. Further investigations of the influence of the base position are presented in the Supporting Information (Figures S6 and S7). At the optimal base position the two modes are best excited with polarization angles of 0° and 90°. The slight detuning from the optimal polarization angle or optimal base position depends on the precise geometry (i.e., top and base length) but is of minor importance due to the small influence. Since we compare T-shaped antennas with varying top and base lengths, we investigate only the resonances at $\varphi = 0°$ and $\varphi = 90°$ without adjusting the base position. These angles are best suited for comparison between different geometries, and the resonances still show a single-mode spectrum. This way, we maintain our simple and intuitive design without losing quality.

Short-Wavelength Resonance (Far-Field Scattering). A huge benefit of the T-shaped antenna is the ease of tailoring both peak resonance wavelengths by changing the two geometry parameters top length t and base length b. Thereby it is important to start with the short-wavelength resonance, which is determined by the top length, since this resonance will not be affected much by changing the base length afterward. Using FDTD simulation, we calculated the resonances for gold dipole gap antennas (T-shaped antennas without the base) and complete T-shaped antennas with a 70 nm long base both with different top lengths t. The light was polarized along the antenna top ($\varphi = 0°$) in both cases. The resonance wavelength in dependence on the top length (t ranging from 50 to 90 nm) is plotted in Figure 4A. The resonance wavelength of both antenna geometries increases linearly with the top length from 650 to 800 nm. This behavior is well known from dipole antenna research.[64] There is only a small blue shift in resonance wavelength between the two types of antenna geometries, and the slope is approximately identical. Experimentally measured resonance wavelengths for a pure dipole antenna and a set of T-shaped antennas are shown as well. As mentioned before, the shift in resonance wavelength between simulation and experiment originates from the imperfection of the inner edges in real fabricated structures. The trends, however, are very similar to each other. In Figure 4B and C we show the measured and calculated scattering spectra for both the pure dipole and the complete T-shaped antenna. For the given fabrication tolerances, simulation and experiment agree well. From the simulation (Figure 4) it can be seen that the peak scattering cross section is slightly smaller for the T-shaped structure. The spectral width of the resonance and therefore the quality factor of the plasmon resonator is hardly affected. We hence have a very flexible means to fix the first resonance wavelength by taking full advantage of the large amount of experience for coupled dipole antennas. For all further investigations, we kept

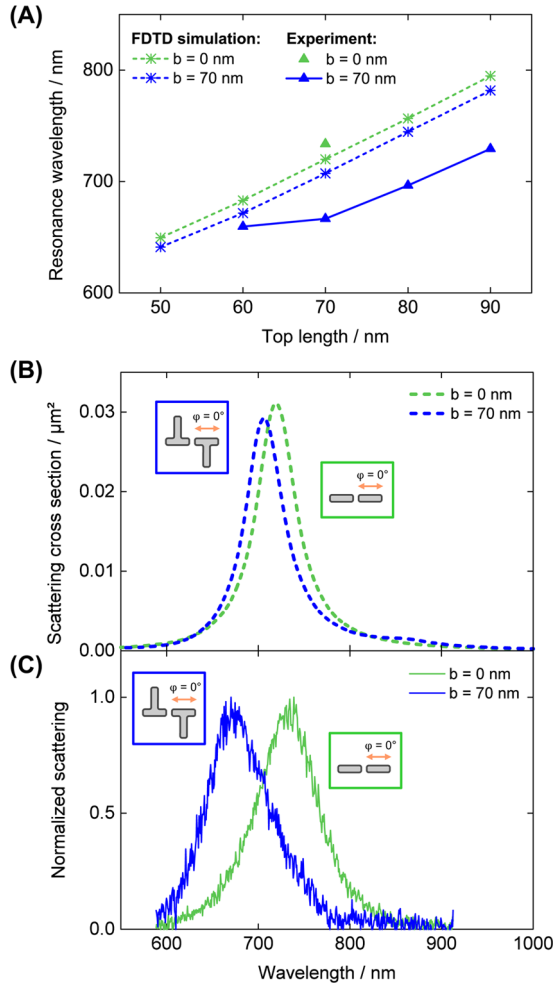

Figure 4. (A) Experimentally obtained (solid line) and simulated (dashed line) resonance wavelengths of dipole nanoantennas (green) and T-shaped antennas (b = 70 nm) (blue) with varying top lengths t to demonstrate the influence of a base on the top resonance. (B) Scattering cross section and (C) normalized scattering of a pure dipole antenna and the top resonance of a coupled T-shaped antenna with a top and base of 70 nm. An attached base results in a blue shift of the resonance wavelength, while the scattering cross section and the resonance shape are hardly influenced.

the top length t fixed at 70 nm and focused on changing the base length b.

Long-Wavelength Resonance (Far-Field Scattering). If a pure dipole antenna is excited with light polarized perpendicular to the long antenna axis, the scattering signal is very low for the investigated wavelength range (Figure 5 top row, magenta lines). Thus, for the experimental conditions given here, we have not observed experimentally any transversal dipole antenna mode. But when the base length becomes significant, a second eigenmode appears in the scattering spectra.

In Figure 5 we further show scattering spectra for T-shaped antennas with a base of 50, 60, 70, and 80 nm length. For these base lengths the base mode is at longer wavelengths than the top mode. In both simulation (dashed lines) and experiment (solid lines) the spectra are shown for a polarization along the top axis ($\varphi = 0°$, blue lines) as well as for a polarization along the base ($\varphi = 90°$, magenta lines). The short wavelength resonances ($\varphi = 0°$) show little dependence on the base length

DOI: 10.1021/acsphotonics.5b00446
ACS Photonics 2015, 2, 1644−1651

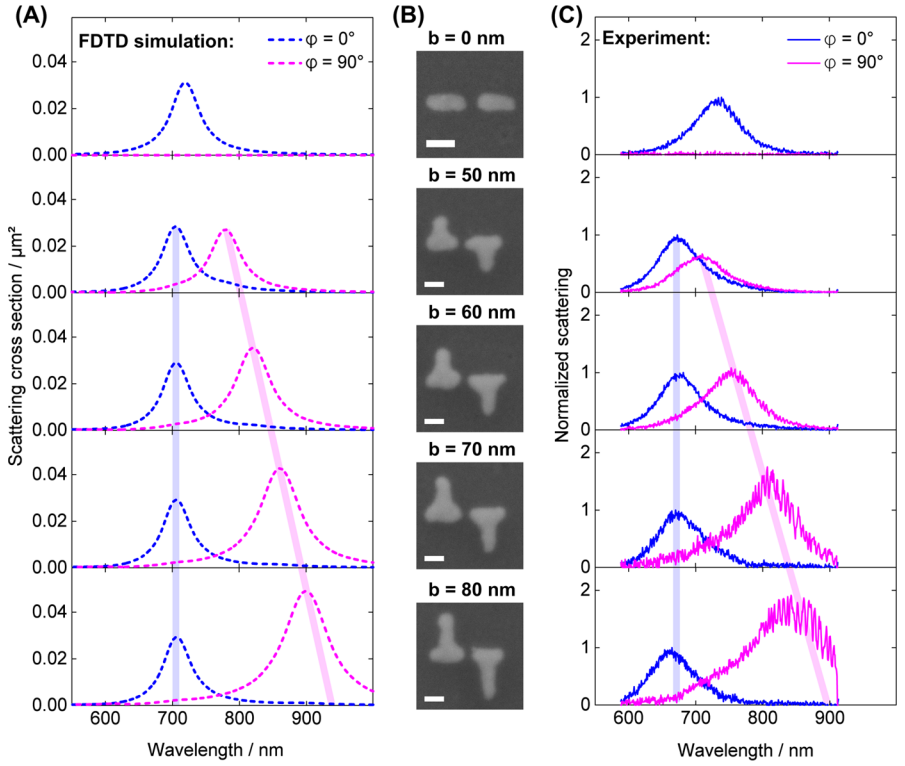

Figure 5. (A) Scattering cross sections from FDTD simulations, (B) SEM images (scale bar 50 nm), and (C) measured normalized scattering via dark-field microscopy of T-shaped antennas with a fixed top length of t = 70 nm and increasing base length (from the top to the bottom row) of b = 0, 50, 60, 70, and 80 nm. The blue color corresponds to the short wavelength top resonance and the magenta color to the long wavelength base resonance. For the dipole only a single mode can be observed. With attached base the second mode appears, and it shifts to longer wavelengths with increasing base lengths. The simulated and measured spectra agree very well (semitransparent lines are guides to the eye).

for both measurements and simulations (Figure 5, blue lines). The simulation results show the absolute scattering cross sections and thus allow for a direct comparison of the resonance amplitudes. Comparing the amplitudes of the short-wavelength resonance for different base lengths among each other, we found that they are nearly constant at about 0.03 μm^2. This finding further reassures that the top mode is not perturbed by changing the base length. Therefore, we normalized each pair (φ = 0°, φ = 90°) of measured spectra to the maximum value of the φ = 0° spectrum. We could then compare the shape and relative magnitude of the two different resonances for each configuration between simulation and experiment. The amplitude ratio between base and top is linearly increasing with increasing base length. Both resonances are well separated by the polarization angle. We can see that the resonance wavelength of the short-wavelength mode (blue lines) is constant at λ_{top} = 707 nm for the simulations and around λ_{top} = 680 nm for the experiments.

When the light is polarized along the antenna base (φ = 90°, magenta lines), the long-wavelength mode of the T-shaped antennas can be observed. For base lengths between 50 and 80 nm, this resonance shifts from 780 nm to 898 nm for the simulations and from 708 nm to 830 nm for the experiments. The resonance wavelength and the relative scattered power also increase with increasing base length. Thus, for a given first eigenmode and a fixed top length, the second mode can be designed to a desired wavelength by adapting the base length without perturbing the first mode heavily.

Figure 6 summarizes how the long-wavelength resonance can be designed without influencing the short-wavelength resonance. Here, the simulations cover a broader range of base

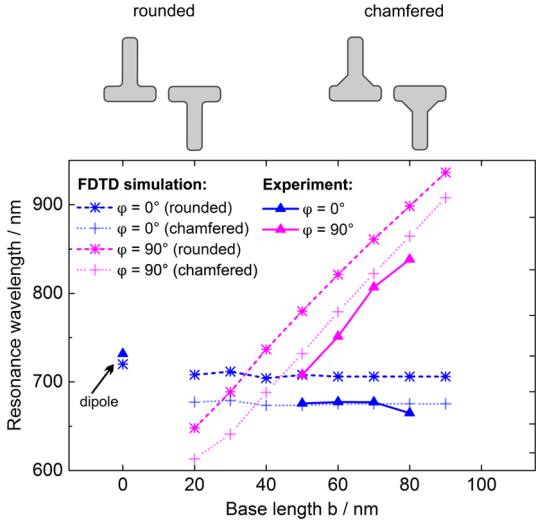

Figure 6. Resonance wavelengths of T-shaped antennas with top length t = 70 nm and different base lengths b for the two polarization angles φ = 0° and φ = 90° extracted from simulations (dashed and dotted lines) and from experiments (solid lines). The two sets of simulation results are for rounded inner edges (left sketch and dashed lines) and for chamfered inner edges (right sketch and dotted lines).

lengths from 20 to 90 nm. For comparison the pure dipole resonance (base length b = 0 nm) is depicted for φ = 0°. It can be seen that configurations exist where the base mode is at shorter wavelengths than the top mode (b = 20 nm to b = 30 nm). However, for these configurations the scattering signal for the base mode is very weak, and we recommend taking the base

DOI: 10.1021/acsphotonics.5b00446
ACS Photonics 2015, 2, 1644−1651

mode as the long-wavelength mode. It is also possible to design an antenna where the two resonance wavelengths are identical, which can also be beneficial for several applications. The long-wavelength resonance shifts linearly and the short-wavelength resonance is constant for both simulation and experiment.

For all simulations so far we rounded all inner and outer edges with a radius of 3 nm (see Methods section), as depicted in the left sketch of Figure 6. It can be seen that the experimental scattering resonances (Figure 6, solid lines) are at shorter wavelengths than the simulated values (Figure 6, dashed lines). This deviation can be mainly assigned to the real shape of the inner edges of the T-structure for the fabricated antennas. The chamfered inner edges are a result of the partly unavoidable proximity effect in electron beam lithography (see SEM images in Figure 5). They lead to a blue shift of the plasmon mode compared to a structure with rounded edges. In Figure 6 (dotted lines) we also included the results from a set of simulations of antennas with chamfered inner edges, as depicted in the right sketch of Figure 6. These particular simulation results agree very well with the experimental results. Hence, we could attribute the major part of the discrepancies between simulated and measured results to the challenge to fabricate sharp inner edges. It can further be seen that this change in geometry is not disadvantageous for the general behavior of the coupled T-shaped antenna geometry and the principles of this work. Even the field enhancement in the gap is only moderately decreased (electric near-field enhancement of the chamfered T-shaped antenna; see Supporting Information, Figures S3 and S4). Since the main focus of our simulations is the understanding of the working principle of T-shaped antennas and not to match them to the experimental results, all other simulations presented in this paper are without chamfered inner edges.

In conclusion, coupled T-shaped optical antennas represent a new class of nanoantennas for applications where two resonant modes are desired. These structures were investigated by numerical simulations, fabricated, and characterized by dark-field scattering experiments. The results clearly show that the structure supports two eigenmodes in the visible-wavelength regime. Both resonances share very high field enhancements in a common subwavelength nanogap. By changing the polarization angle, the first, the second, or both eigenmodes can be excited. We showed that the resonance modes can be easily and independently tuned to desired wavelengths by selecting a specific length of the top and the base of the T-shaped antenna. Such structures combined with QEs in the electromagnetic hot spot enable a promising way to fully control single-photon sources. Beyond this, a multitude of further bimodal applications can benefit from this coupled T-shaped antenna structure.

METHODS

Experiments. The coupled T-shaped gold nanoantennas were reproducibly fabricated with electron beam lithography (eLINE, Raith) on a 30 nm indium tin oxide (ITO)-covered glass coverslip. A diluted PMMA 950k resist with a resulting layer thickness of 62 nm was used, and the exposure was performed with 10 kV high voltage. After exposure and development a 30 nm thick gold layer was thermally evaporated, and finally a lift-off process in acetone was performed. Scanning electron microscopy (SEM) was used to verify the success of the lithography process and to identify the best fabrication parameters such as exposure dose and development time. For the SEM analysis a representative set of nanoantennas was used to avoid contamination of the antennas that are further used for the optical characterization. Both the nanoantennas for the SEM and those for the optical characterization were fabricated on the same substrate by using exactly the same electron beam lithography procedure.

To characterize the optical properties of the fabricated T-shaped antennas, we performed single-particle dark-field scattering spectroscopy in transmission mode. We used an inverted microscope (Axio Observer, Zeiss) with attached spectrometer (Spectra Pro 2500i, Princeton Instruments) and electron multiplying charge coupled device (EMCCD) camera (Andor iXon, Andor Technologies) to obtain scattering spectra of individual nanoantennas. A linear polarization filter in the detection path allowed us to select specific polarization angles. The polarization filter maintains an extinction ratio between 10^6 and 10^8 over the operating bandwidth. A halogen lamp with a broad spectrum and a color temperature of 3200 K was used as excitation source, and the sample was illuminated via a dark-field condenser (NA = 1.2, Leitz Wetzlar). The spectra of the scattered light at the nanoparticles were normalized by subtracting the background close to the antenna from the detected signal and dividing it by the optical transfer function of the system and the spectrum of the excitation source for each polarization, respectively. The peak resonances were determined with a Lorentzian fit to the measured resonance spectra.

Simulations. The antenna structures were theoretically studied using FDTD method based numerical simulations.[65] In this model, a plane wave was incident on an individual gold antenna structure on an ITO-covered glass substrate. The polarization angle φ of the plane wave was varied as indicated in the paper. The wave was injected from the glass substrate side, which was considered to be infinitely large and thick for these simulations. The ITO layer had a thickness of 30 nm. The optical constants for the gold antenna structures (taken from the paper of Johnson and Christy[66]) as well as for the ITO layer (in-house ellipsometry measurement data; see Supporting Information Figure S7) were frequency dependent, while the glass substrate was modeled with a constant refractive index of $n = 1.5$. Corners and edges of the gold nanostructure were rounded by a radius of 3 nm to avoid unrealistic high field enhancements at sharp edges within the simulation results. We used a fine mesh with a spatial resolution of 0.625 nm for each dimension for the nanostructure and its close proximity. The mesh gradually became coarser toward the outer borders of the simulation area. A region of 800 nm × 800 nm × 800 nm surrounded by 24 perfectly matched layers ensured that the finiteness of the simulation area did not affect the results. The scattered power flowing through a closed box that surrounds the antenna was integrated and normalized by the incident intensity, giving us the scattering cross sections. As near-field parameters we investigated the electric field distributions in the plane at half the antenna height for the resonance wavelengths. Finally, also the current density distribution at half the antenna height for specific wavelengths was calculated.

ASSOCIATED CONTENT

Supporting Information

The Supporting Information is available free of charge on the ACS Publications website at DOI: 10.1021/acsphotonics.5b00446.

DOI: 10.1021/acsphotonics.5b00446
ACS Photonics 2015, 2, 1644−1651

Spectral properties of the near-field enhancement in the gap; electric field vectors in the gap; influences of chamfered inner edges on the near-field; FDTD simulations of the angle dependence on the two modes with mathematical fit; influence of the base position; in-house ellipsometry measurement data of the optical constants for ITO (PDF)

AUTHOR INFORMATION

Corresponding Authors

*E-mail: katja.dopf@kit.edu.
*E-mail: carola.moosmann@kit.edu.
*E-mail: hans.eisler@kit.edu.

Author Contributions

‡K. Dopf and C. Moosmann contributed equally to this work and are co-first authors.

Notes

The authors declare no competing financial interest.

ACKNOWLEDGMENTS

C.M., K.D., and P.M.S. thank the Karlsruhe School of Optics and Photonics (KSOP) for general support. P.M.S. further thanks the Helmholtz International Research School for Teratronics (HIRST).

REFERENCES

(1) Mühlschlegel, P.; Eisler, H.-J.; Martin, O. J. F.; Hecht, B.; Pohl, D. W. Resonant optical antennas. *Science* **2005**, *308*, 1607−1609.
(2) Bharadwaj, P.; Deutsch, B.; Novotny, L. Optical antennas. *Adv. Opt. Photonics* **2009**, *1*, 438−483.
(3) Novotny, L.; van Hulst, N. Antennas for light. *Nat. Photonics* **2011**, *5*, 83−90.
(4) Biagioni, P.; Huang, J.-S.; Hecht, B. Nanoantennas for visible and infrared radiation. *Rep. Prog. Phys.* **2012**, *75*, 024402.
(5) Agio, M., Alù, A., Eds. *Optical Antennas*; Cambridge University Press, 2013.
(6) Dahmen, C.; Schmidt, B.; von Plessen, G. Radiation damping in metal nanoparticle pairs. *Nano Lett.* **2007**, *7*, 318−322.
(7) Nordlander, P.; Oubre, C.; Prodan, E.; Li, K.; Stockman, M. I. Plasmon hybridization in nanoparticle dimers. *Nano Lett.* **2004**, *4*, 899−903.
(8) Aizpurua, J.; Bryant, G. W.; Richter, L. J.; García De Abajo, F. J.; Kelley, B. K.; Mallouk, T. Optical properties of coupled metallic nanorods for field-enhanced spectroscopy. *Phys. Rev. B: Condens. Matter Mater. Phys.* **2005**, *71*, 235420.
(9) Halas, N. J.; Lal, S.; Chang, W.-S.; Link, S.; Nordlander, P. Plasmons in strongly coupled metallic nanostructures. *Chem. Rev.* **2011**, *111*, 3913−3961.
(10) Atwater, H. A.; Polman, A. Plasmonics for improved photovoltaic devices. *Nat. Mater.* **2010**, *9*, 205−213.
(11) Knight, M. W.; Sobhani, H.; Nordlander, P.; Halas, N. J. Photodetection with active optical antennas. *Science* **2011**, *332*, 702−704.
(12) Wang, F.; Melosh, N. A. Plasmonic energy collection through hot carrier extraction. *Nano Lett.* **2011**, *11*, 5426−5430.
(13) Schlather, A. E.; Large, N.; Urban, A. S.; Nordlander, P.; Halas, N. J. Near-field mediated plexcitonic coupling and giant rabi splitting in individual metallic dimers. *Nano Lett.* **2013**, *13*, 3281−3286.
(14) Yuan, C. T.; Wang, Y. C.; Cheng, H. W.; Wang, H. S.; Kuo, M. Y.; Shih, M. H.; Tang, J. Modification of fluorescence properties in single colloidal quantum dots by coupling to plasmonic gap modes. *J. Phys. Chem. C* **2013**, *117*, 12762−12768.
(15) Ming, T.; Chen, H.; Jiang, R.; Li, Q.; Wang, J. Plasmon-controlled fluorescence: beyond the intensity enhancement. *J. Phys. Chem. Lett.* **2012**, *3*, 191−202.
(16) Kinkhabwala, A.; Yu, Z.; Fan, S.; Avlasevich, Y.; Müllen, K.; Moerner, W. E. Large single-molecule fluorescence enhancements produced by a bowtie nanoantenna. *Nat. Photonics* **2009**, *3*, 654−657.
(17) Farahani, J. N.; Eisler, H.-J.; Pohl, D. W.; Pavius, M.; Flückiger, P.; Gasser, P.; Hecht, B. Bow-tie optical antenna probes for single-emitter scanning near-field optical microscopy. *Nanotechnology* **2007**, *18*, 125506.
(18) Kauranen, M.; Zayats, A. V. Nonlinear Plasmonics. *Nat. Photonics* **2012**, *6*, 737−748.
(19) Suh, J. Y.; Odom, T. W. Nonlinear properties of nanoscale antennas. *Nano Today* **2013**, *8*, 469−479.
(20) Canfield, B. K.; Husu, H.; Bai, B.; Laukkanen, J.; Kuittinen, M.; Turunen, J.; Kauranen, M. Second-harmonic generation driven by asymmetric local fields in T-shaped gold nanodimers. *Proc. SPIE* **2007**, *6641*, 66410Q.
(21) Kauranen, M.; Husu, H.; Canfield, B. K.; Laukkanen, J.; Bai, B.; Kuittinen, M.; Turunen, J. P. Gap-dependent chiral coupling in T-shaped gold nanodimers. *Proc. SPIE* **2008**, *6988*, 69880K.
(22) Aouani, H.; Navarro-Cia, M.; Rahmani, M.; Sidiropoulos, T. P. H.; Hong, M.; Oulton, R. F.; Maier, S. A. Multiresonant broadband optical antennas as efficient tunable nanosources of second harmonic light. *Nano Lett.* **2012**, *12*, 4997−5002.
(23) Husu, H.; Siikanen, R.; Mäkitalo, J.; Lehtolahti, J.; Laukkanen, J.; Kuittinen, M.; Kauranen, M. Metamaterials with tailored nonlinear optical response. *Nano Lett.* **2012**, *12*, 673−677.
(24) Thyagarajan, K.; Rivier, S.; Lovera, A.; Martin, O. J. F. Enhanced second-harmonic generation from double resonant plasmonic antennae. *Opt. Express* **2012**, *20*, 12860−12865.
(25) Celebrano, M.; Wu, X.; Baselli, M.; Großmann, S.; Biagioni, P.; Locatelli, A.; De Angelis, C.; Cerullo, G.; Osellame, R.; Hecht, B.; Duò, L.; Ciccacci, F.; Finazzi, M. Mode matching in multiresonant plasmonic nanoantennas for enhanced second harmonic generation. *Nat. Nanotechnol.* **2015**, *10*, 412−417.
(26) Czaplicki, R.; Mäkitalo, J.; Siikanen, R.; Husu, H.; Lehtolahti, J.; Kuittinen, M.; Kauranen, M. Second-harmonic generation from metal nanoparticles: resonance enhancement versus particle geometry. *Nano Lett.* **2015**, *15*, 530−534.
(27) Chettiar, U. K.; Engheta, N. Optical frequency mixing through nanoantenna enhanced difference frequency generation: metatronic mixer. *Phys. Rev. B: Condens. Matter Mater. Phys.* **2012**, *86*, 075405.
(28) Biagioni, P.; Savoini, M.; Huang, J. S.; Duò, L.; Finazzi, M.; Hecht, B. Near-field polarization shaping by a near-resonant plasmonic cross antenna. *Phys. Rev. B: Condens. Matter Mater. Phys.* **2009**, *80*, 153409.
(29) Biagioni, P.; Wu, X.; Savoini, M.; Ziegler, J.; Huang, J.-S.; Duò, L.; Finazzi, M.; Hecht, B. Tailoring the interaction between matter and polarized light with plasmonic optical antennas. *Proc. SPIE* **2011**, *7922*, 79220C.
(30) Trevino, J.; Walsh, G. F.; Pecora, E. F.; Boriskina, S. V.; Dal Negro, L. Photonic-plasmonic-coupled nanoantennas for polarization-controlled multispectral nanofocusing. *Opt. Lett.* **2013**, *38*, 4861−4863.
(31) Yang, J.; Zhang, J. Subwavelength quarter-waveplate composed of L-shaped metal nanoparticles. *Plasmonics* **2011**, *6*, 251−254.
(32) Biagioni, P.; Huang, J. S.; Duò, L.; Finazzi, M.; Hecht, B. Cross resonant optical antenna. *Phys. Rev. Lett.* **2009**, *102*, 256801.
(33) Kumar, V. D.; Bhardwaj, A.; Mishra, D. Investigation of a turnstile nanoantenna. *Micro Nano Lett.* **2011**, *6*, 94−97.
(34) Zhang, Z.; Weber-Bargioni, A.; Wu, S. W.; Dhuey, S.; Cabrini, S.; Schuck, P. J. Manipulating nanoscale light fields with the asymmetric bowtie nano-colorsorter. *Nano Lett.* **2009**, *9*, 4505−4509.
(35) Shegai, T.; Chen, S.; Miljković, V. D.; Zengin, G.; Johansson, P.; Käll, M. A bimetallic nanoantenna for directional colour routing. *Nat. Commun.* **2011**, *2*, 481.
(36) Yang, Y. Y.; Zhang, Y. L.; Jin, F.; Dong, X. Z.; Duan, X. M.; Zhao, Z. S. Steering the optical response with asymmetric bowtie 2-color controllers in the visible and near infrared range. *Opt. Commun.* **2011**, *284*, 3474−3478.

DOI: 10.1021/acsphotonics.5b00446
ACS Photonics 2015, 2, 1644−1651

(37) Luk'yanchuk, B.; Zheludev, N. I.; Maier, S. A.; Halas, N. J.; Nordlander, P.; Giessen, H.; Chong, C. T. The Fano resonance in plasmonic nanostructures and metamaterials. *Nat. Mater.* **2010**, *9*, 707−715.
(38) Xi, Z.; Lu, Y.; Yu, W.; Wang, P.; Ming, H. Improved sensitivity in a T-shaped nanodimer plasmonic sensor. *J. Opt.* **2013**, *15*, 025004.
(39) Binfeng, Y.; Guohua, H.; Jiawei, C.; Yiping, C. Fano resonances induced by strong interactions between dipole and multipole plasmons in T-shaped nanorod dimer. *Plasmonics* **2014**, *9*, 691−698.
(40) Panaro, S.; Nazir, A.; Liberale, C.; Das, G.; Wang, H.; De Angelis, F.; Proietti Zaccaria, R.; Di Fabrizio, E.; Toma, A. Dark to bright mode conversion on dipolar nanoantennas: a symmetry-breaking approach. *ACS Photonics* **2014**, *1*, 310−314.
(41) Panaro, S.; Nazir, A.; Liberale, C.; Wang, H.; De Angelis, F.; Proietti Zaccaria, R.; Di Fabrizio, E.; Toma, A. Dark and bright modes manipulation for plasmon-triggered photonic devices. *Proc. SPIE* **2014**, *9163*, 91633M.
(42) Kim, K.-H.; Kim, S.-H.; Bae, M.-C. Fano resonance by dipole - hexapole coupling in a χ -shaped plasmonic nanostructure. *Appl. Opt.* **2015**, *54*, 2710−2714.
(43) Simovski, C.; Morits, D.; Voroshilov, P.; Guzhva, M.; Belov, M.; Kivshar, Y. Enhanced efficiency of light-trapping nanoantenna arrays for thin-film solar cells. *Opt. Express* **2013**, *21*, A714−A725.
(44) Voroshilov, P. M.; Simovski, C. R.; Belov, P. A. Nanoantennas for enhanced light trapping in transparent organic solar cells. *J. Mod. Opt.* **2014**, *61*, 1743−1748.
(45) Sinev, I. S.; Voroshilov, P. M.; Mukhin, I. S.; Denisyuk, A. I.; Guzhva, M. E.; Samusev, A. K.; Belov, P. A.; Simovski, C. R. Demonstration of unusual nanoantenna array modes through direct reconstruction of the near-field signal. *Nanoscale* **2015**, *7*, 765−770.
(46) Harutyunyan, H.; Volpe, G.; Quidant, R.; Novotny, L. Enhancing the nonlinear optical response using multifrequency gold-nanowire antennas. *Phys. Rev. Lett.* **2012**, *108*, 217403.
(47) Lu, G.; Liu, J.; Zhang, T.; Shen, H.; Perriat, P.; Martini, M.; Tillement, O.; Gu, Y.; He, Y.; Wang, Y.; Gong, Q. Enhancing molecule fluorescence with asymmetrical plasmonic antennas. *Nanoscale* **2013**, *5*, 6545−6551.
(48) Aouani, H.; Šípová, H.; Rahmani, M.; Navarro-Cia, M.; Hegnerová, K.; Homola, J.; Hong, M.; Maier, S. A. Ultrasensitive broadband probing of molecular vibrational modes with multifrequency optical antennas. *ACS Nano* **2013**, *7*, 669−675.
(49) Yang, J.; Kong, F.; Li, K.; Sheng, S. Analysis of a log periodic nano-antenna for multi-resonant broadband field enhancement and the Purcell factor. *Opt. Commun.* **2015**, *342*, 230−237.
(50) Yang, J.; Zhang, J. Nano-polarization-converter based on magnetic plasmon resonance excitation in an L-shaped slot antenna. *Opt. Express* **2013**, *21*, 7934−7942.
(51) Gao, Z.; Wang, Z.-Y. Terahertz plasmonic cross resonant antenna. *J. Electromagnet. Wave.* **2011**, *25*, 1730−1739.
(52) Ünlü, E. S.; Tok, R. U.; Sendur, K. Broadband plasmonic nanoantenna with an adjustable spectral response. *Opt. Express* **2011**, *19*, 1000−1006.
(53) Stokes, J. L.; Yu, Y.; Yuan, Z. H.; Pugh, J. R.; Lopez-Garcia, M.; Ahmad, N.; Cryan, M. J. Analysis and design of a cross dipole nanoantenna for fluorescence-sensing applications. *J. Opt. Soc. Am. B* **2014**, *31*, 302−310.
(54) Farahani, J. N.; Pohl, D. W.; Eisler, H.-J.; Hecht, B. Single quantum dot coupled to a scanning optical antenna: A tunable superemitter. *Phys. Rev. Lett.* **2005**, *95*, 017402.
(55) Kühn, S.; Håkanson, U.; Rogobete, L.; Sandoghdar, V. Enhancement of single-molecule fluorescence using a gold nanoparticle as an optical nanoantenna. *Phys. Rev. Lett.* **2006**, *97*, 017402.
(56) Cohen-Hoshen, E.; Bryant, G. W.; Pinkas, I.; Sperling, J.; Bar-Joseph, I. Exciton-plasmon interactions in quantum dot-gold nanoparticle structures. *Nano Lett.* **2012**, *12*, 4260−4264.
(57) Taminiau, T. H.; Stefani, F. D.; Segerink, F. B.; van Hulst, N. F. Optical antennas direct single-molecule emission. *Nat. Photonics* **2008**, *2*, 234−237.
(58) Kosako, T.; Kadoya, Y.; Hofmann, H. F. Directional emission of light from a nano-optical Yagi-Uda antenna. *Nat. Photonics* **2010**, *4*, 312−315.
(59) Curto, A. G.; Volpe, G.; Taminiau, T. H.; Kreuzer, M. P.; Quidant, R.; van Hulst, N. F. Unidirectional emission of a quantum dot coupled to a nanoantenna. *Science* **2010**, *329*, 930−933.
(60) Giannini, V.; Sánchez-Gil, J. A. Excitation and emission enhancement of single molecule fluorescence through multiple surface-plasmon resonances on metal trimer nanoantennas. *Opt. Lett.* **2008**, *33*, 899−901.
(61) Wissert, M. D.; Schell, A. W.; Ilin, K. S.; Siegel, M.; Eisler, H.-J. Nanoengineering and characterization of gold dipole nanoantennas with enhanced integrated scattering properties. *Nanotechnology* **2009**, *20*, 425203.
(62) Prangsma, J. C.; Kern, J.; Knapp, A. G.; Grossmann, S.; Emmerling, M.; Kamp, M.; Hecht, B. Electrically connected resonant optical antennas. *Nano Lett.* **2012**, *12*, 3915−3919.
(63) Menzel, C.; Hebestreit, E.; Mühlig, S.; Rockstuhl, C.; Burger, S.; Lederer, F.; Pertsch, T. The spectral shift between near- and far-field resonances of optical nano-antennas. *Opt. Express* **2014**, *22*, 9971−9982.
(64) Novotny, L. Effective wavelength scaling for optical antennas. *Phys. Rev. Lett.* **2007**, *98*, 266802.
(65) Lumerical Solutions, Inc., 2015; www.lumerical.com.
(66) Johnson, P. B.; Christy, R. W. Optical constants of the noble metals. *Phys. Rev. B* **1972**, *6*, 4370−4379.

DOI: 10.1021/acsphotonics.5b00446
ACS Photonics 2015, 2, 1644−1651